One-Way Nested Grid Models: The Interface Conditions and the Numerical Accuracy

K. MIYAKODA AND A. ROSATI

Geophysical Fluid Dynamics Laboratory/NOAA, Princeton University, Princeton, N.J. 08540

(Manuscript received 1 February 1977, in revised form 2 May 1977)

ABSTRACT

Tests of several interface conditions in a one-way nested grid model were undertaken, where the ratio of grid size for the coarse mesh in the large domain and the fine mesh in the small domain was 4:1. The interface values for all parameters are specified by the solutions of the larger domain model, although they are modified in some cases. Scheme A includes a "boundary adjustment" and the consideration of mountain effect for the surface pressure along the interface. Scheme B uses, in addition to Scheme A, a "radiation condition" at the outward propagation boundaries. Scheme C uses viscous damping along five rows adjacent to the border lines in addition to Scheme A. The solutions for the fine-mesh models obtained by these schemes are compared quantitatively with the solution of a control model. The results show how quickly the effect at the interface propagates into the interior. The proper treatment of the mountain effect on the surface pressure along the interface, and the boundary adjustment are important for obtaining reasonable solutions. Schemes A, B and C are all acceptable, though not entirely satisfactory. Scheme B was useful in reducing the false reflection at the interface. Scheme C gave smooth fields of predicted variables, but false reflection sometimes occurred. A combination of these conditions optimally chosen was applied to a 34 km mesh model for a domain covering the whole mainland of the United States. The resulting maps of the time integration show the formation of a front and the detailed structure of intense rainbands associated with the front.

1. Introduction

In the 1950's, the papers by Reed and Sanders (1953), Reed and Danielsen (1959) and Newton (1954) pointed out a fascinating and intriguing fact of the intense concentration of vorticity along a frontal zone. The width of the zone, in which the large potential temperature gradient and the intense vorticity are confined, is very narrow (~100 km). The location of the zone is closely related to the jet stream at the subtropical tropopause gap. This vorticity concentration has recently been reexamined observationally, theoretically and numerically (e.g., Shapiro and Hastings, 1973; Williams, 1967; Eliassen and Raustein, 1968; Hoskins and Bretherton, 1972; Bleck, 1973); its existence as well as its dynamical significance have been confirmed.

Associated with the front, cyclogenesis or the development of larger scale disturbances are often observed, the horizontal scale of the frontal waves being ~1000–2000 km. It is the current understanding in linear perturbation theory (e.g., Simons, 1972; Gall, 1976) that under a typical distribution of zonal mean basic flow, the dynamical instability due to the baroclinicity as well as the horizontal wind shear activates perturbations of first the zonal wavenumbers 12–15 (~2000 km), and thereafter, wavenumbers 5–9 (~6000 km).[1]

[1] However, the recent study by Simmons and Hoskins (1976) has given a somewhat different picture.

It is likely, therefore, that adequate resolution of the structure of the narrowly confined vorticity and the accurate determination of its behavior are important and instrumental for improved prediction of frontal waves and ultimately for the precise simulation of the growth of baroclinic waves. In fact, Bushby and Timpson (1967) and Benwell *et al.* (1971) in the United Kingdom, and Matsumoto *et al.* (1970), Gambo (1970) and Nitta and Ogura (1972) in Japan, have already paid a great deal of attention to these disturbances. Bleck (1974) also made an extensive test on the prediction of these scales with an isentropic model.

The scale of these disturbances are the meso-α (250–2000 km) and the macro-β (2000–10 000 km), according to Orlanski's (1975) nomenclature. In order to treat and resolve these classes of meteorological systems with a numerical model, a grid size of ~10–50 km seems to be required. In view of the limitation of the computing capacity at present or even in the foreseeable future, however, it is reasonable to handle this type of problem with a regional area model rather than with a global or hemispheric model. This restriction necessitates an adequate scheme for nesting of small and large domain models to maintain the interior solution accurate for a considerable span of time.

Previously, along this line of thought, a number of studies have been made (Hill, 1968; Wang and Halpern, 1970). We also (Chen and Miyakoda, 1974; hereafter

refer to as CM) discussed the interface nesting condition for a barotropic free surface (two-dimensional shallow water equation) model. The present paper is the extension of CM to the three-dimensional case. The limited domain covers the entire mainland of the United States with the grid size of $\sim$34 km. The two objectives of this paper are 1) to test the numerical accuracy of the nesting interface conditions and 2) to describe the preliminary results of the performance by the nested grid model with the full physics.

2. Prelude

There are a number of ways of formulating interface conditions for the nested grid model. Perhaps it is difficult at present to conclude definitively which method is the most appropriate and superior in the calculation of the meso-α scale weather systems. The current status of the problems and the techniques in fine-mesh modeling was summarized by Elsberry (1975) (though the major portion of that paper was devoted to the discussion of the hurricane nested model). There are two general approaches, i.e., models of one-way and two-way nesting between the interior and the exterior (or the large area) meshes. In the present paper, we will use exclusively the one-way approach, in which the boundary conditions for the interior are prescribed by external data taken from the larger domain and not the reverse.

Elvius and Sundström (1973) and CM discussed the well-posed interface conditions for the one-way nesting problem.[2] In CM, two schemes of the interface conditions were recommended for the shallow water equation, i.e., the first method (the Dirichlet conditions with local boundary smoothing) and the second method (the well-posed conditions). In the present model, we will use interface conditions which are basically of the first method type. For the barotropic model, these conditions are as follows.

All variables u, v and ϕ (the velocity vectors and the height of water) are provided by the solutions from the large area coarse mesh at all boundary points. Therefore, the boundary data vary with time. Interpolations in time and space are used whenever necessary, and this is an overspecification of the boundary condition. However, the strain resulting from the overspecification is considerably relaxed in the case of nesting, because the external data are almost compatible with the equations of the interior in the dynamical characteristics. In addition, the strain is further alleviated, when "boundary adjustment" (smoothing) is applied. The boundary adjustment is used only to the grid points next to the boundary. This process serves to link together different modes of computational solutions. The adjustment algorithm for u at the west boundary, for example, is

$$\bar{\bar{u}}_2=\tfrac{1}{2}u_2+\tfrac{1}{4}(u_1+u_3), \tag{2.1}$$

where $\bar{\bar{u}}$ is the adjusted data, and the suffixes 1, 2 and 3 are the indices of the grid points counted from the boundary. Note that this adjustment is applied in the direction normal to the boundary only.

This scheme was actually applied to the "GFDL 1967 version general circulation model" (Smagorinsky *et al.*, 1965) which was originally built in 1963 (Manabe *et al.*, 1965) as the hemispheric general circulation model, and was utilized for the prediction model (Miyakoda, 1973). It consists of nine vertical levels and used the primitive equations of motions, the thermodynamics equation, and the continuity equation in which u, v, T (temperature), q (the mixing ratio of water vapor) and p_s (the surface pressure) are adopted as prognostic variables. The physics involved are dry convective adjustment, longwave and shortwave radiation, large-scale condensation of water vapor, ensemble cumulus convection represented by moist convective adjustment, nonlinear viscosity, surface drag, sensible heat flux and evaporation from the earth's surface, and vertical turbulent transfer in the planetary boundary layer modeled by the eddy viscosity method. Topography Z^* is included and the variables are specified at σ-surfaces, where $\sigma=p/p_s$ (Phillips, 1957). The surface temperature over the land is determined by a heat budget at the ground surface, whereas the sea-surface temperature and the temperature over sea-ice are specified. The equations are defined on the stereographic projection map. The finite-difference equations are the kinetic energy conservation scheme, and the time differencing is the leapfrog method with intermittent time-level averaging.

One deviation of the present model from the 1967 version is the usage of a time filter (Robert, 1966; Asselin, 1972) instead of the Euler-backward scheme. This is mainly because the former is easier to handle in the nesting boundary condition. For the fine- and coarse-mesh domains, the same model was used with different grid sizes. Therefore, the meteorological variables carried in both models and the vertical levels are the same. The large domain is the hemispheric extension bounded by the equator, and the small domain is the regional rectangular area which will be described shortly.

Fig. 1 illustrates the interface between the coarse-mesh large domain and the fine-mesh small domain. The coarse grid points are represented by circles, and the fine grid points by small dots; the numbers are attached for convenience of explanation. The interface lines, for example, are 5–6 and 5–14. All variables at the coarse grid points 5, 7, 14, etc., are given at the large time interval Δt_1. Using these data, the values at the interface lines for the fine-mesh points such as 6 and 10 are obtained by linear interpolation in time, where the time interval is $\Delta t_2=\Delta t_1/4$.

[2] See also the recent report of Oliger and Sundström (1976) for some of the basic problems on boundary condition.

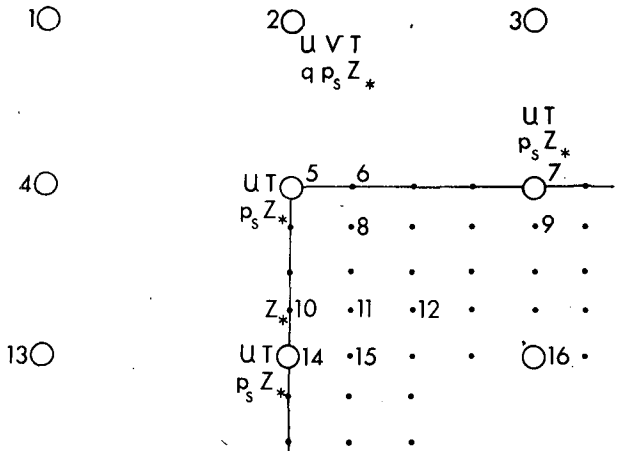

FIG. 1. The interface zone between the coarse and the fine meshes: open dots are coarse grid point, solid dots fine grid points.

3. Interface conditions

Several major aspects of the interface conditions will be discussed. In order to provide all the interface data, horizontal interpolation has to be made. We used Shapiro's (1970) first-order (four-point) interpolation scheme. Let us denote the data along the boundary interpolated in time and space by $\hat{u}$, $\hat{v}$, $\hat{T}$, $\hat{q}$ and $\hat{p}_s$.

a. The mountain effect

As mentioned earlier, we employed the nesting method of CM, but for the first experiment only, the "boundary adjustment" was not incorporated. The solution in the limited domain turned out quite noisy, mostly because the hydrostatic equilibrium was not properly maintained associated with the mountains along the boundary. As a remedy, a new surface pressure (p_s) was calculated so that the hydrostatic equilibrium was satisfied. There are two schemes to obtain p_s as follows:

1) The horizontal interpolation is made for T, q, z (geopotential height), u and v on the pressure (p) surface [u and v could be better interpolated on θ-surfaces (Shapiro and Hastings, 1973)]. Then p_s at the interface (e.g., point 6 in Fig. 1) is calculated hydrostatically as $p_s=f(\hat{T}, \hat{q}, \hat{Z}, Z^*)$, using $dZ=-(R/g)T_v d(\ln p)$, where Z^* is the topography of the fine mesh, T_v the virtual temperature, g the acceleration of gravity and R the gas constant of dry air.

2) The horizontal interpolation is made for T, z, u, v, p_s and Z^* on the σ-surface. Then a correction for the difference $\hat{Z}^*-Z^*$ is added to $\hat{p}_s$ hydrostatically by the formula $p_s=\hat{p}_s[1+(g/R\hat{T}_v)\times(\hat{Z}^*-Z^*)]$, where $\hat{Z}^*$ is the interpolated topographic height from the large domain's mountain.

The former method is more precise, but we currently employ the latter method, which is substantially simpler.

b. The boundary adjustment

If one uses the boundary condition with p_s hydrostatically adjusted as described above, the excessive spurious generation of gravity waves at the boundaries is appreciably reduced, and the solutions in the limited domain are much smoother. Yet the solutions still appear to contain a considerable amount of wiggling. The cause of this is mainly the adoption of the non-staggered grid [Scheme A in the classification of Arakawa and Mintz (1974)], partly due to the time-differencing scheme and also due to the overspecification as was mentioned in CM. In order to reduce the degree of separation of two computational modes, the boundary adjustment is applied for the next row of variables every time step just after the forecast calculation in the small domain is finished [Wang and Halpern (1970) used a similar scheme].

For example, ϕ at point 11 in Fig. 1 is calculated by (2.1), where ϕ is any of u, v, T, q, p_s and Z^*. For u and v, the calculation can be made on the σ-surface, but T and q have to be calculated on the p- or z-surfaces at three grid points, i.e., 10, 11 and 12. The surface pressure p_s at 11 is then obtained by $p_s=\hat{p}_s[1+(g/R\hat{T}_v)(\hat{Z}^*-Z^*)]$.

c. The radiation condition

With the above scheme, the solutions in the limited domain sometimes still show a computational mode; apparently false reflection occurs at the boundary. This problem, associated with the interface conditions, has already been pointed out by Elvius and Sundström (1973).

In order to overcome this difficulty, the "radiation condition" seems to form a useful extrapolation procedure. The idea is to allow interior disturbances to pass through the lateral boundary, if directed outward, and not to allow reflection at the interface. The treatment we adopted in this paper was devised by Orlanski (1976); the method was successfully used for the open boundary case in some barotropic one-dimensional test problems.

Historically speaking, Wurtele *et al.* (1971) studied Sommerfeld's far-field radiation condition from a different angle in connection with the open boundary treatment. Shapiro and O'Brien (1970) and Williamson and Browning (1974) used horizontal Lagrangian trajectories of particles from the exterior to the interface for determining the boundary values if the coarse-mesh winds are directed out of the small domain.

The radiation condition is written, for an arbitrary variable ϕ, by

$$\frac{\partial \phi}{\partial t}+mc\frac{\partial \phi}{\partial n}=0, \tag{3.1}$$

where n is the coordinate normal to the boundary, c the propagation speed of the wave and m the map-scale

factor (Kreiss, 1968; Pearson, 1974). It is noteworthy that only a derivative in the direction normal to the boundary is included and that all coupling between the variables is neglected. In other words, this equation is used not only for one-dimensional but also for two- and three-dimensional cases. The scheme appears considerably simpler than the "one-sided method" or the "characteristic method." In Orlanski's method, the propagation speed c is estimated from the numerical values of ϕ at the neighboring grid points. It is thus not necessary to have a knowledge of the theoretical formula of the phase speed beforehand.

Using the ϕ's at the various time levels, τ, $\tau-1$ and $\tau-2$, one can obtain at the eastern boundary, for example, from (3.1)

$$c=-\left[\frac{\phi^{\tau}(JM-1)-\phi^{\tau-2}(JM-1)}{\frac{1}{2}[\phi^{\tau}(JM-1)+\phi^{\tau-2}(JM-1)]-\phi^{\tau-1}(JM-2)}\right]\times\frac{1}{m(JM-1)}\left(\frac{\Delta s}{2\Delta t}\right), \quad (3.2)$$

where Δs is the grid size, Δt the time interval, JM the index of grid at the boundary, and $(JM-1)$ and $(JM-2)$ denote the next and second next grid point to the boundary. In the case $c>0$, the disturbance propagates outward through the boundary which we call the "outward propagation boundary." In the case $c<0$, it is the inward propagation boundary. In the former case, if $c>\Delta s/\Delta t$, c is set to be equal to $\Delta s/\Delta t$, and if $\Delta s/\Delta t>c>0$, then c in (3.2) is used as it is.

Thus, the boundary values of ϕ at $\tau+1$ is given by

$$\phi^{\tau+1}(JM)=\frac{[1-(\Delta t/\Delta s)cm(JM)]}{[1+(\Delta t/\Delta s)cm(JM)]}\phi^{\tau-1}(JM)+\frac{2(\Delta t/\Delta s)cm(JM)}{[1+(\Delta t/\Delta s)cm(JM)]}\phi^{\tau}(JM-1). \quad (3.3)$$

On the other hand, in the case of the inward propagation, the solutions of the coarse-mesh models are simply prescribed at the boundary.

The propagation speed c is in general different for each parameter at each level. It is worth mentioning that the evaluation of c was done on the z-surface for p_s and on p-surfaces for T instead of σ-surfaces. The second method in CM discriminated the inflow and outflow boundaries. Strictly speaking, the discrimination should be done depending upon the inward or outward propagation boundaries rather than the inflow or outflow boundaries. In Orlanski's "radiation condition," the idea is to construct a simple interface condition that is close to the one used in the second method of CM, i.e., it should at least let the dominating waves of the solution pass through the boundary without reflection. Thus, summarizing the above, a determination is first made for each variable whether the propagation is inward or outward, and second, *if inward, the variable is specified by the exterior solution, and if outward, the condition (3.3) is used.*

d. The "sponge" (the viscous damping)

The second technique we adopted is the "sponge" treatment used by Bushby and Timpson (1967), Kessel and Winninghoff (1972), Williamson and Browning (1974), Burridge (1975) and others, and in a somewhat different way by Kreitzberg *et al.* (1974) and Perkey and Kreitzberg (1976). In order to suppress the noise, highly dissipative boundaries are posed to damp the gravity waves at the interface when generated, and absorb disturbances when they propagate from the interior to the vicinity of the interface. The computational modes or other incompatibility between the interface condition and the fine-mesh model are all dissipated by a strong viscous damping (lateral diffusion), which is applied to the rows of the grid along the interior of the boundary, excluding the interface row. This treatment is applied, superimposed upon the first method of CM. (This technique is ingenious, extremely simple, straightforward and accordingly easy to implement. It is, however, our view that this is a, so-to-speak, "brute force" method, which might overly suppress not only noise but also significant information, and may be considered inelegant. Thus, our original intention was to minimize the usage of this technique.)

e. Remarks

Hovermale (personal communication), Anthes (1974) and Davies (1976) proposed the "Newtonian damping" method for the interface condition; this is mathematically reminiscent of the "Newtonian radiational cooling" and is also a simple, brute force method. We tested this in our case. Although the result is not shown here, the quality seems similar to (or somewhat worse than) the "sponge damping."

There are a number of devices to yield a smooth interface such as the geostrophic balance in the boundary condition mentioned by Jones (1974), the adequate determination of the normal component of velocity to control the gravity wave in the interface zone used by Okamura (1975), the prescription of the time rate of change in the tangential velocities extrapolated from the interior employed by Burridge (1975), and the control of noise generation with orthogonally oriented calculation of divergence by Mesinger (1973) and Mesinger and Janjič (1974). This scheme is apparently only effective in the particular lattice system they used, i.e., Scheme E in the classification of Arakawa and Mintz (1974). Obviously, it is not our objective to survey exhaustively all damping methods associated with the nesting, but a scheme which we have not tested and appears attractive is that proposed by Sasaki (1970).

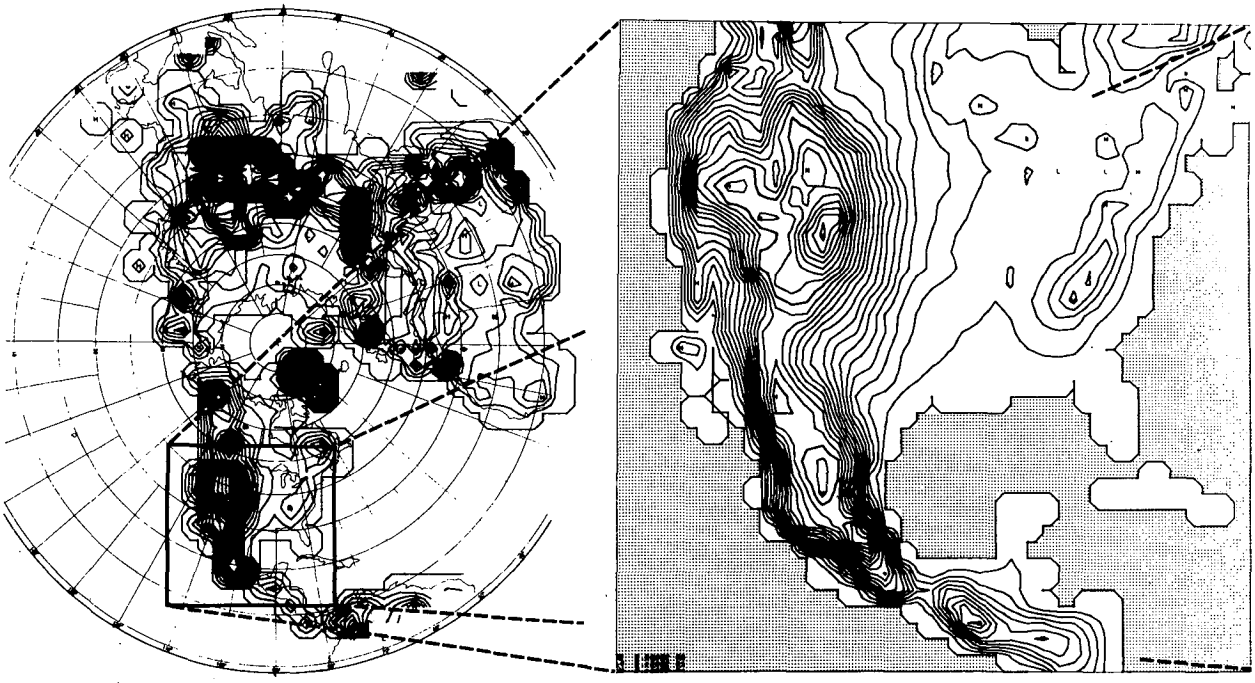

FIG. 2. The large (hemispheric) domain and the small domain. The contour interval for the topography is 120 m.

The method is to force smoothness in some selected parameters, while maintaining the "best" possible agreement of the solution with the forecast equations in the context of variational principle.

4. Design of tests

The first objective of this paper is to test the validity and the numerical accuracy of the formulations of interface condition. One way of evaluating the accuracy is to prepare the solutions of the everywhere-fine-mesh model for a sufficiently wide domain and to compare the solutions of the proposed nested models with the former solution. This approach was taken in CM, although the system of equations was much simpler. After several years of preparation we are now in a position to do the same with the three-dimensional full physics model.

a. The grid resolution

All the models appearing in this section have the Cartesian coordinate grid on the stereographic projection map. The same grid was previously used in Miyakoda *et al.* (1971), in which the domain covered the entire hemisphere. The grid resolution in that case was called $N20$, $N40$ or $N80$, where N is the number of grid points between the pole and equator; $N40$, for example, means that there are 40 pole–equator points in the entire domain. In this paper, we will follow this custom of identification of the resolution, though N is in this case the number of grid points between the center and the edge of the rectangular domain instead of the pole-equator grid points.

We use two hemispheric models as references.

$N80$: Reference 1, $\Delta s = 135$ km

$N20$: Reference 2, $\Delta s = 540$ km.

The values of the grid size Δs are for mid-latitudes. Reference 1 (Ref. 1) is the control solution, which are the target (or goal) in the comparison test. Ref. 2 is the lowest level of standard; the solution of any useful nested model should be better than Ref. 2.

In this section only, for the small area, the $N20$ model will be used exclusively. The grid size of this $N20$ model is 1/4 of Ref. 2. This means that the grid points for the limited domain are exactly the same as that of Ref. 1. Let us denote $N20$ (1/4) as this type of $N20$ model; the domain is, therefore, $(1/4)^2$ of the large domain (if one includes the corners) (see Fig. 2). The small rectangular area is located over the mainland of the United States. In Fig. 2, the topography is also shown. We first specified the $N80$ topography, and then the $N20$ topography was determined by selecting every fourth point from the $N80$ topography.

We then define two systems of the nested grid as

- $N80/N20(1/4)$: used for calibration
  $\Delta s_1 = 135$ km and $\Delta s_2 = 135$ km
- $N20/N20(1/4)$: used for test of nested models
  $\Delta s_1 = 540$ km and $\Delta s_2 = 135$ km.

Here Δs_1 and Δs_2 are the grid sizes for the large and small domain models, respectively. The system $N80/N20(1/4)$ consists of the $N80$ model for the large domain and the $N20(1/4)$ model for the small domain. This means that the grid ratio is 1:1. If no interface

arrangement is done for the $N20(1/4)$ model, the solution of the limited domain becomes exactly identical with that of Ref. 1, within the accuracy of roundoff error. Therefore, this system is trivial, but the numerical test with this system is useful and even indispensable for the calibration of the coupled system of the two models. As was mentioned above, however, this type of interface condition does not work in the case of (even slightly) different mesh sizes. That is why we need the interface device, and it is indeed the reason for the usage of the nesting scheme.

The system $N20/N20(1/4)$ uses the $N20$ model for the large domain and the $N20(1/4)$ model for the small domain; the grid ratio is, therefore, 4:1. This was the system primarily used for the tests in this paper.

b. Initial conditions and verification data

It is not the intent of this paper to design an elaborate initialization procedure for the nested grid system. In order to avoid the complexity of this problem and yet to allow the precise comparison of various models, we took a short-cut approach to the initial conditions. First a marching calculation with the $N80$ model was carried out for about 10 days with $\Delta t_2 = 2.5$ min, using the hemispheric data set valid at 1200 GMT 14 March 1965, as the starting time. We then chose 1200 GMT 18 March as the initial time $\tau = 0$ for the present tests. Ref. 1 is simply the solutions of the $N80$ model mentioned above.

The initial data for Ref. 2 was taken from the original $N80$ run at $\tau_2 = 0$ and -4, which correspond to $\tau_1 = 0$ and -1, respectively, for the $N20$ model run, where τ_1 and τ_2 are the time level indices for the coarse and fine meshes, respectively (the leapfrog calculation requires two time levels of data.) From this data set, the values at every fourth grid point were picked up so as to match spatially the $N20$ grid. Ref. 2 ran with $\Delta t_1 = 10$ min. The initial conditions for the $N20(1/4)$ runs are the same as that for Ref. 1 valid at 1200 GMT 18 March, as $\tau_2 = 0$: the only difference is that the integration domain is limited.

c. Various systems

In the formulation of interface condition, we have included a number of artifices to suppress unfavorable effects, i.e., the "hydrostatic adjustment," the "boundary adjustment," the "radiation condition," the "time filter" and the "sponge." With combinations of these processes, we constructed A-, B- and C-systems (later D-system) of the models. In all cases, the $N20/N20(1/4)$ configuration was used. The boundary data were derived from the $N20$ hemispheric model. The only exception is that in the Y-model the exterior data were taken from Ref. 1; however, the nesting scheme is exactly the same as that of A-system (this is not the calibration any more).

Each version of the nested model is specified below.

- *A-system (= Y-system)*:

  The simplest scheme, i.e., the hydrostatic adjustment along the boundary, the boundary adjustment and the time filter.

- *B-system:*

  The A-system scheme plus the radiation condition.

- *C-system:*

  The A-system scheme plus the sponge with the strong lateral viscosity along five rows of buffer zone adjacent to the interface. The viscosity coefficient is 25 times larger than the usual value of the nonlinear viscosity coefficient.

Before proceeding to the discussion on the results by these systems, we will demonstrate how each individual process of the noise reduction operates. We made a preliminary test with the purposely degraded models as follows.

A-system minus the hydrostatic adjustment
A-system minus the boundary adjustment
A-system minus the time filter
C-system minus the boundary adjustment.

Fig. 3 is an example of the geopotential height at 500 mb level for the 0.5th day from the beginning of the forecast. The maps for A-system minus the hydrostatic adjustment clearly indicate wiggles at the mountain regions along the interface. This error propagated toward interior and contaminated the entire region rapidly. The effectiveness of the boundary adjustment is pronounced in these figures. The sponge treatment does not control the difficulty without the boundary adjustment as seen in the comparison of the A- and C-models. The 2-grid oscillation is particularly evident. The boundary adjustment is most effectively applied to p_s, but an experiment showed that the additional application of the boundary adjustment to other variables gave even smoother patterns.

The effect of the time filter may be seen in the comparison of maps in the A-model and that in the A minus time-filter model. This effect is not large, though noticeable. Thus we feel that the processes seem to be important in the following order: the hydrostatic equilibrium along the boundary, the boundary adjustment, the sponge effect and the time filter.

5. Results of comparison: Maps

The individual maps of the experiments for the selected parameters during the 2-day forecast period will be shown. Ref. 1, Ref. 2, A, B, C and Y models were chosen, and the maps will be displayed in the manner as shown in Fig. 4. Figs. 5, 6 and 7 are the maps for the temperature $T7$ at the seventh σ-level ($\sim$811 mb), the

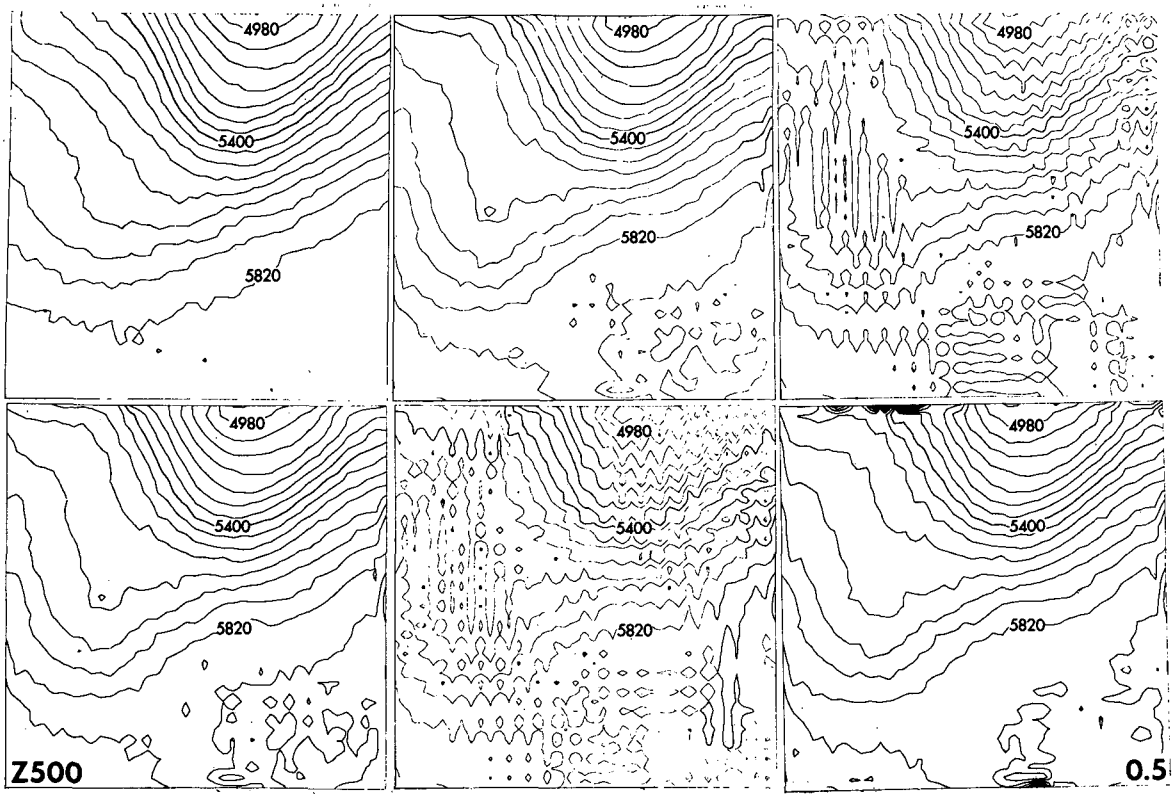

FIG. 3. The geopotential height Z at the 500 mb level for 0.5 day (contour interval 60 m). Upper: Ref. 1 (left) A-model minus time filter (middle), C-model minus boundary adjustment (right). Lower: A-model (left), A-model minus boundary adjustment (middle), A-model minus hydrostatic adjustment (right).

y-component $V9$ of wind at the ninth σ-level ($\sim$991 mb) and the rate of precipitation (rain). Neither smoothing nor filtering were applied to the output except the built-in time filter and the subgrid-scale turbulent viscosities in the prediction models as well as the aforementioned interface techniques.

We first look at the overall features, comparing the maps of models with those of Refs. 1 and 2. The following may be observed.

1) The patterns of $T7$ and $V9$ for Ref. 2 are very smooth, whereas those for Ref. 1, A, B, C and Y have small-scale disturbances. Most of these small-scale features in A, B, C and Y seem to correspond to those in Ref. 1, indicating that the detailed structures are not random noise but significant signals.

Ref 1 N80	B	A
Y	C	Ref 2 N20

FIG. 4. Layout of the maps in Figs. 5, 6 and 7.

2) The merit of the refined-resolution model is noticeable in all parameters, in the sense that A, B, C and Y are closer to Ref. 1 than Ref. 2 is to Ref. 1. The advantage is appreciable, in the following order, for the parameters of rain, $V9$ and $T7$.

3) The similarity of the Y model to Ref. 1 is outstanding except for a considerable discrepancy at the mountains of Central America along the interface.

It may be interesting to note that the A-, B- and C-systems give fair results, though the patterns in C-system tend to be excessively smooth in comparison with Ref. 1 not only in the border regions but also in the central areas. The fact of the false reflection at the northeast interface in A, B and C would deserve particular attention. These spurious reflections in day 2 for $T7$ in A and C, and at the east boundary in day 2 for $V9$ in A and C are striking. The reflected waves propagated back and on day 3 were located in the middle of the domain in the maps $T7$ (not shown here). On the other hand, B-model handled this problem better, as was expected. The maps are not shown here, but $Z500$, for example, shows very clearly the false reflection of disturbances in A and C but not in B.

However, even in B the wiggles as a consequence of

the false reflection had not been entirely eliminated. The reason for the incomplete removal is probably that the phase speed calculated was valid only for one portion of the wave spectrum and that we neglected the coupling between the different variables, and accordingly, all waves were not entirely advected out through

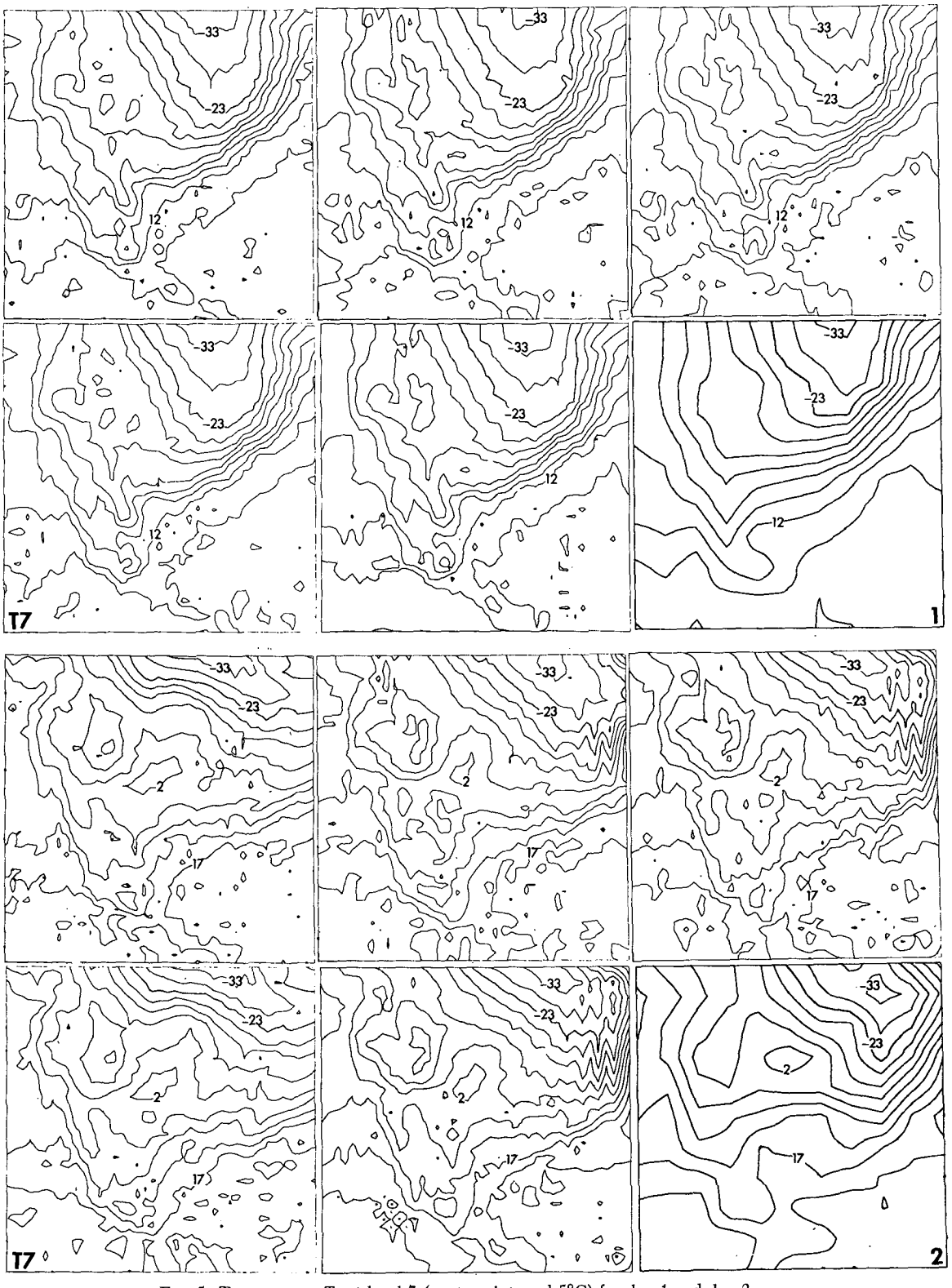

FIG. 5. Temperature T_7 at level 7 (contour interval 5°C) for day 1 and day 2.

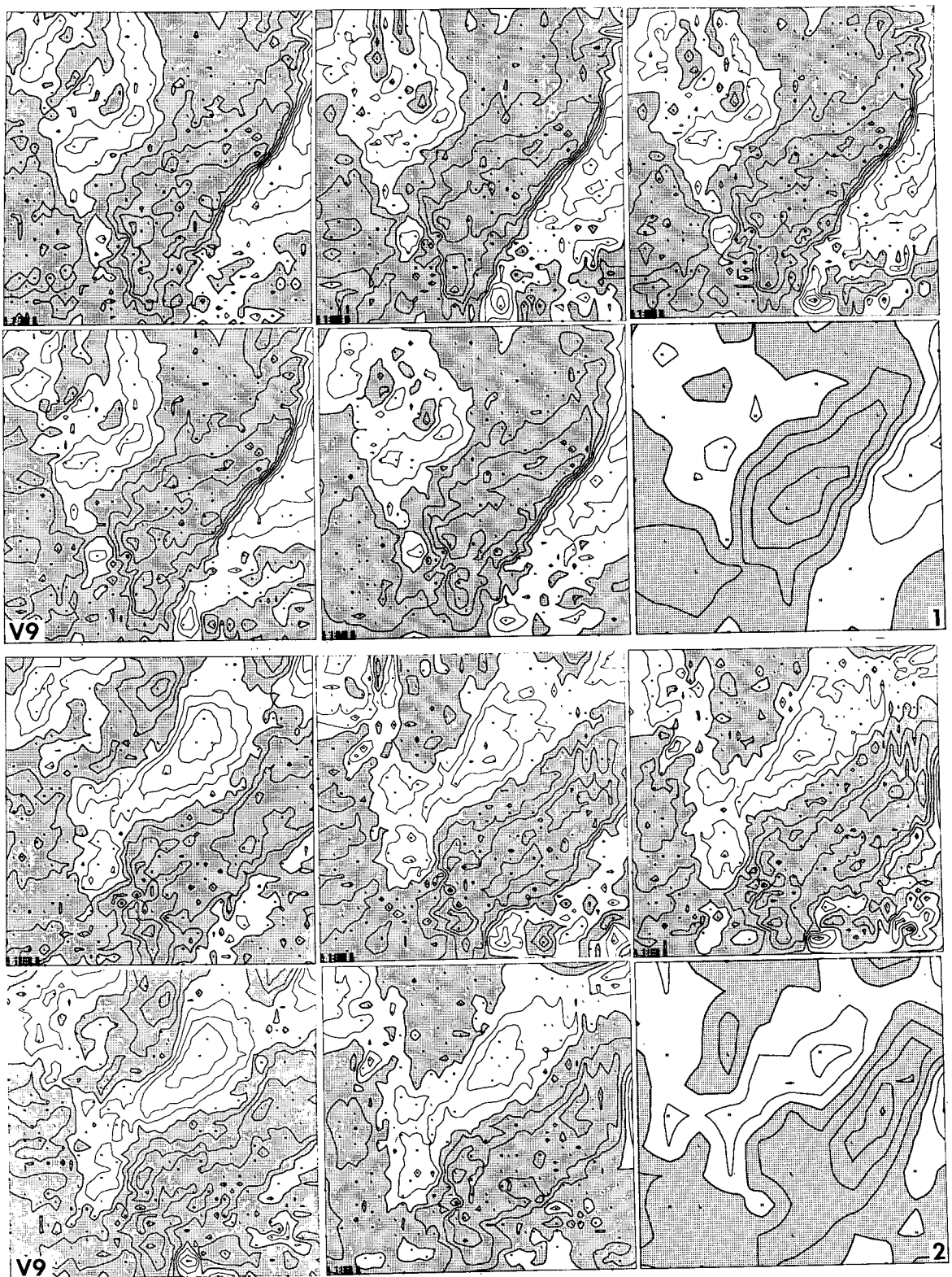

FIG. 6. The y-component of wind (V_9) at level 9 (contour interval 5 m s^{-1}) for day 1 and 2. The negative regions are shaded.

the interface. The fact that the Y-model has a good solution and the A-model has a large error suggests that the error comes mostly from the erroneous values at the interface. Interestingly, the false reflection was also considerably (in practice entirely) alleviated in the case of the Y-model.

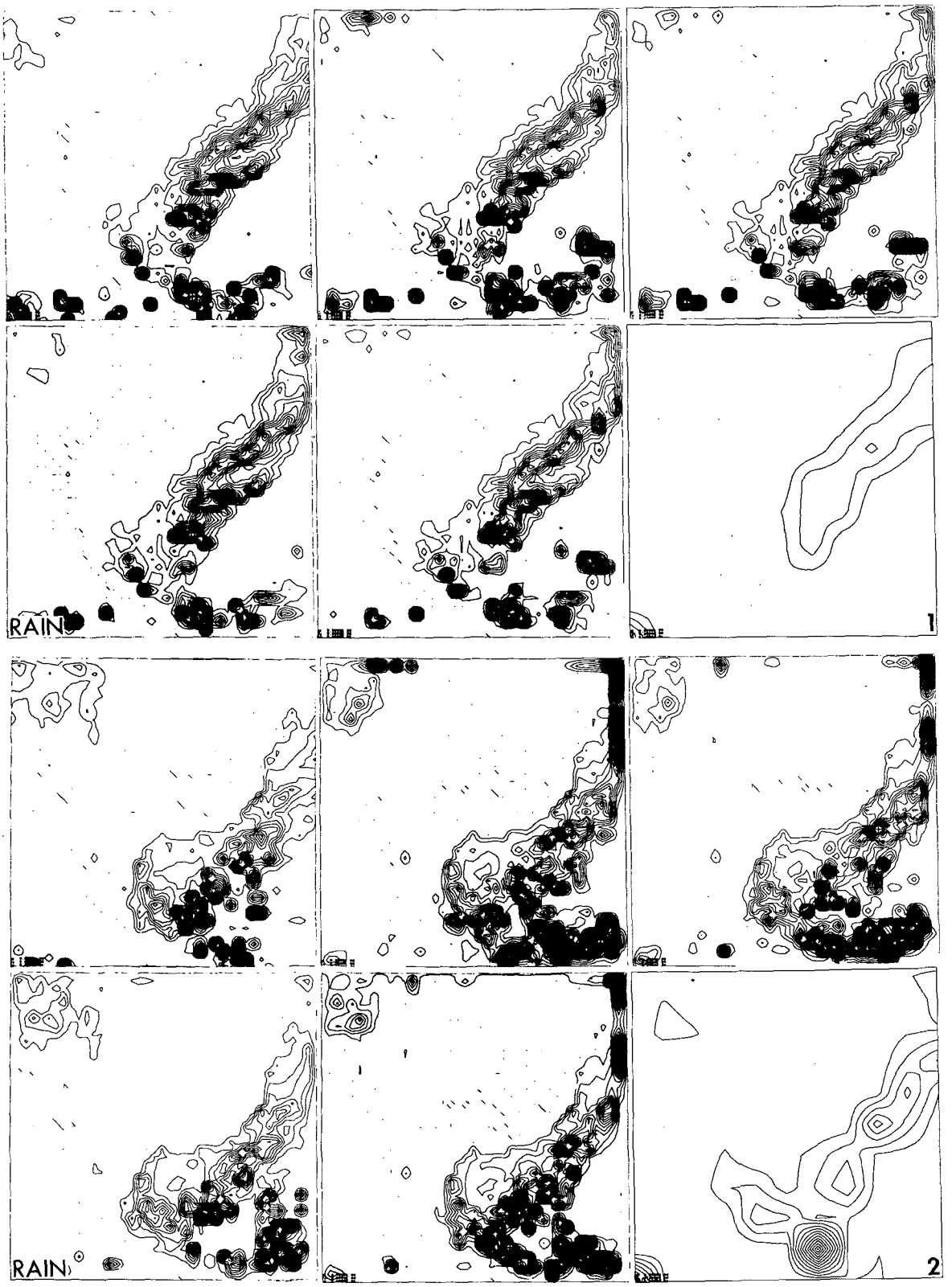

FIG. 7. Rate of precipitation (rain), contour interval 9.8 cm day^{-1} for day 1 and day 2.

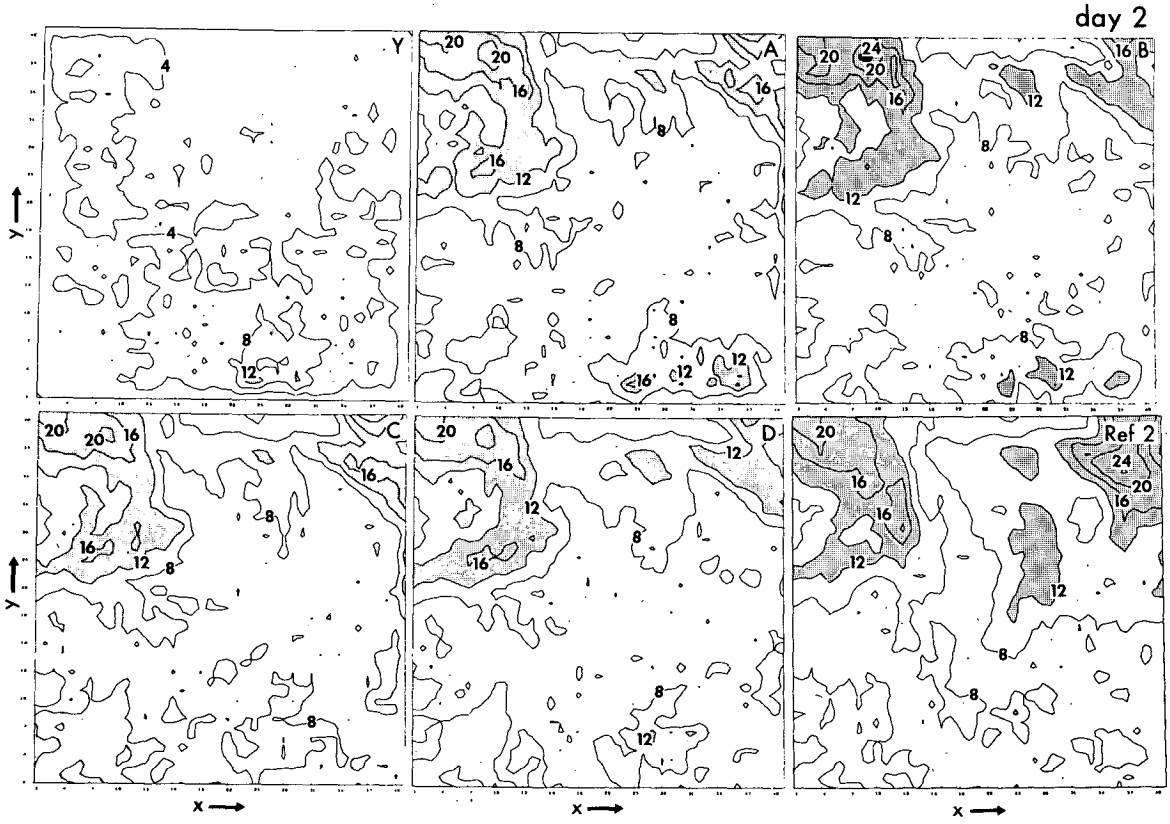

FIG. 8. Distributions of wind errors (m s^{-1}) vertically integrated for models Y, A, B, C, D and Ref. 2 at day 2. The areas in which the error is larger than 12 m s^{-1} are shaded.

6. Numerical accuracy

Since we consider Ref. 1 as the target, the deviation of the solution in other systems from that of Ref. 1 is defined as the error. Fig. 8 presents the horizontal distribution of the wind errors for six systems of the model, i.e., Y, A, B, C, D and Ref. 2 for day 2, where D-system is a combination of Schemes B and C. The values are the vertically integrated rms error of wind; the shaded areas indicate the regions of large wind error. The errors are small in all models for the day 1 but they grow quickly beyond 2 days. The major source of error comes from the interface data at the west and east boundaries. All errors in A, B, C, D and Y are smaller than those in Ref. 2.

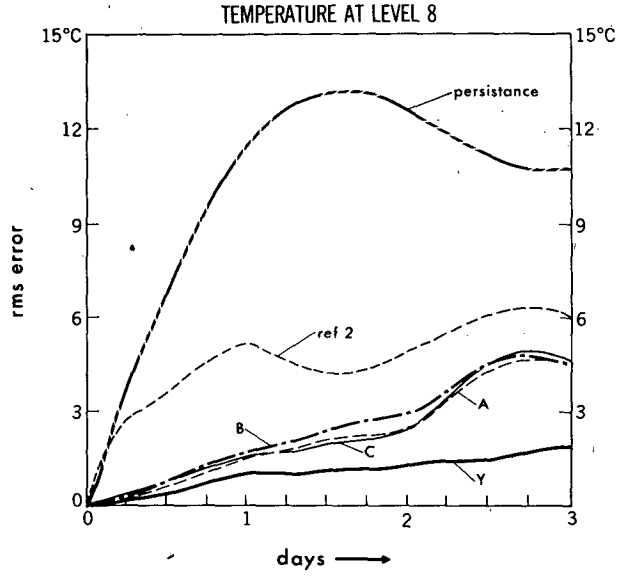

FIG. 9. Evolution of temperature errors at level 8 for models Y, A, B, C, D and Ref. 2. Persistence is also shown.

In particular, the error of Y is extremely small compared with the errors of other models. In Y, the first error starts at the high terrain of the southern interface, suggesting that the model atmosphere is sensitive to tropical mountains, and also indicating that treatment of mountains in this paper turned out to have some shortcomings. The difficulty seems to be caused from the "boundary adjustment" associated with σ-levels.

Another noteworthy point is that the error eventually became large overall in the middle latitudes. It may be of some interest that the error associated with the mountains along the interface is small in the interface buffer region in C and D; the sponge apparently absorbed the unfavorable noise including errors. It is somewhat surprising that B-system has a relatively

large error, perhaps because the radiation condition did not quite treat all kinds of disturbances. The false reflection of disturbances gave an unpleasant look, and yet does not show up appreciably in the rms error.

Fig. 9 shows the curves of the error growth for temperature at the eighth σ-level. The error of Y-model remained small for the entire 3 days. The errors in A, B and C are significantly smaller than Ref. 2 up to 2 days, and became appreciable at 3 days.

Concerning the error distribution in the vertical (Fig. 10), the rms errors of the A-model stayed at the relatively small values in comparison with the error in Ref. 2 in the lower part of the atmosphere, whereas the 1 day. This is understandable, since only the horizontally large-scale disturbances dominate in the stratosphere, and these are not advantageous for the limited domain model. In other words, the merit of the nested grid model can only be obtained for the lower part of the atmosphere and not the upper part.

In order to gain a clearer picture of the error growth, we prepared Fig. 11 in which the wind errors integrated vertically are plotted as a function of x and t. The quantity was calculated for the C-model and Ref. 2 at intervals of 0.25 day from 0.25 to 3 days.

It is most pronounced that the error distribution and its development are similar overall to both the C-model and Ref. 2, but the magnitude in the C-model is substantially smaller than that in Ref. 2. The invasion and growth of error are rapid; the left half of the limited domain is appreciably contaminated in 2 days. It is worthy to note that even at 3 days, the C-model has less error than Ref. 2, which is also shown in Fig. 9. Once the error is generated in the region, it then develops due to dynamic instability. These errors eventually approach an asymptotic distribution which the atmospheric dynamics intrinsically determine.

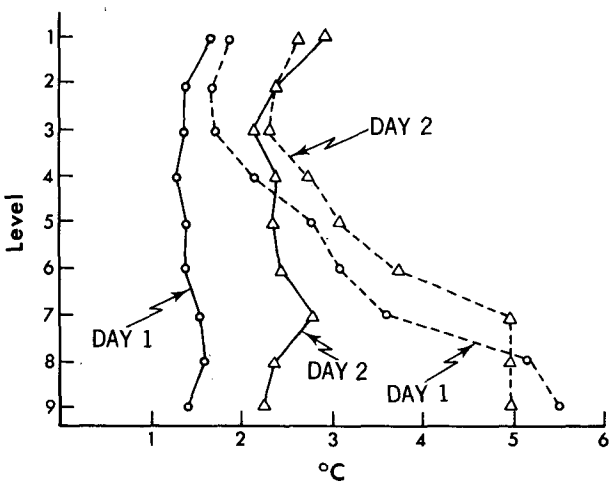

FIG. 10. Vertical distribution of rms error of temperature in C-model (solid lines) and Ref. 2 (dashed lines) for days 1 and 2.

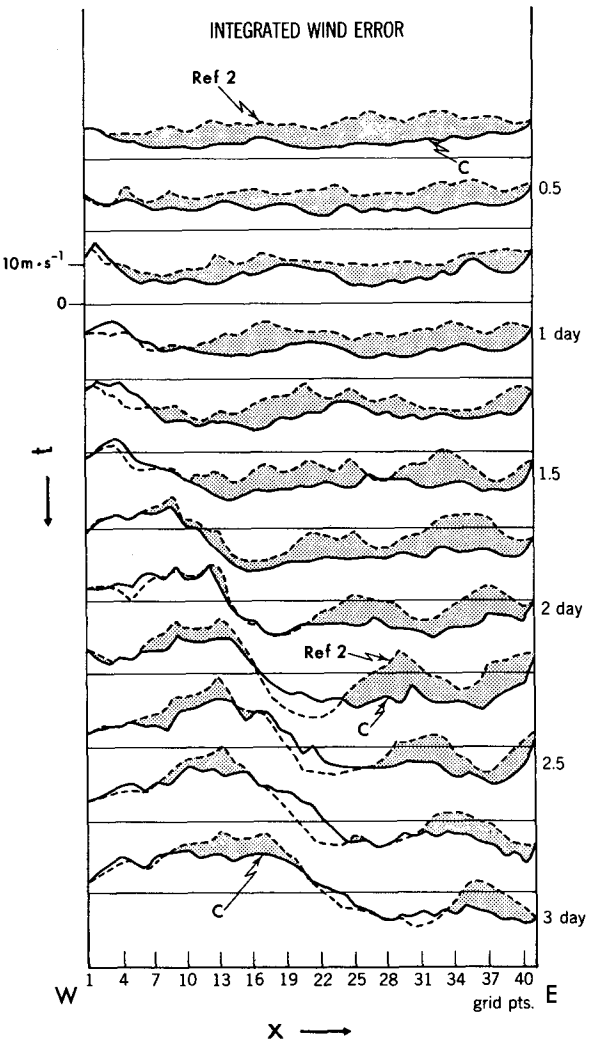

FIG. 11. Wind error (rms) integrated vertically as a function of x and t. The solid lines are the errors of C-model, and the dashed lines those of Ref. 2. The parts in which the error of C-model is smaller than that of Ref. 2 are shaded.

The 34 km grid model

The D-model was applied to the $N80/N80(1/4)$ grid system with nine vertical levels. The limited domain is the same as that used in the previous sections, which covers the entire mainland of the United States. Therefore, the limited domain of $N80(1/4)$ has about 34 km grid size, whereas the hemispheric model of $N80$ resolution has 135 km grid size at the middle latitude (see Table 1). The initial conditions for the $N80(1/4)$ model were obtained by interpolation of the original $N80$ run over the desired region, and the topography was created in the same manner.

In order to demonstrate the efficiency of the nested grid, the three systems of various grid size are compared, i.e., $N80/N80(1/4)$, $N80$ and $N20$. The grid ratios are 1:4:16 and the computing times required for each model are listed in Table 1. In order to calculate

TABLE 1. Relative computing times for each model.

	*N*20	*N*80	*N*320*	*N*80/*N*80(1/4)
Time ratio	1	64	4096	320
Grid size	540 km	135 km	34 km	34 km

* Theoretical.

the fine-mesh model with the grid size of 34 km for the entire hemisphere, the time required is 4096 times of that used by the hemispheric *N*20 model. On the other hand, the nested model of *N*80/*N*80(1/4) requires only 320 times that of the *N*20. By the way, the early nested grid model by Kaplan and Paine (1973) has a grid system of 127 km×32 km and 10*L*/9*L* for the coarse/fine meshes which is close to the present system in this paper. Their coarse-mesh model is quasi-geostrophic and the fine-mesh model is the primitive equations, and the small domain has 36 km×32 km grid points.

Returning to the numerical results in our study, we look at Fig. 12, in which the predicted maps at day 1 for the three grid systems are shown. In this particular case, the initial conditions were the same as were used

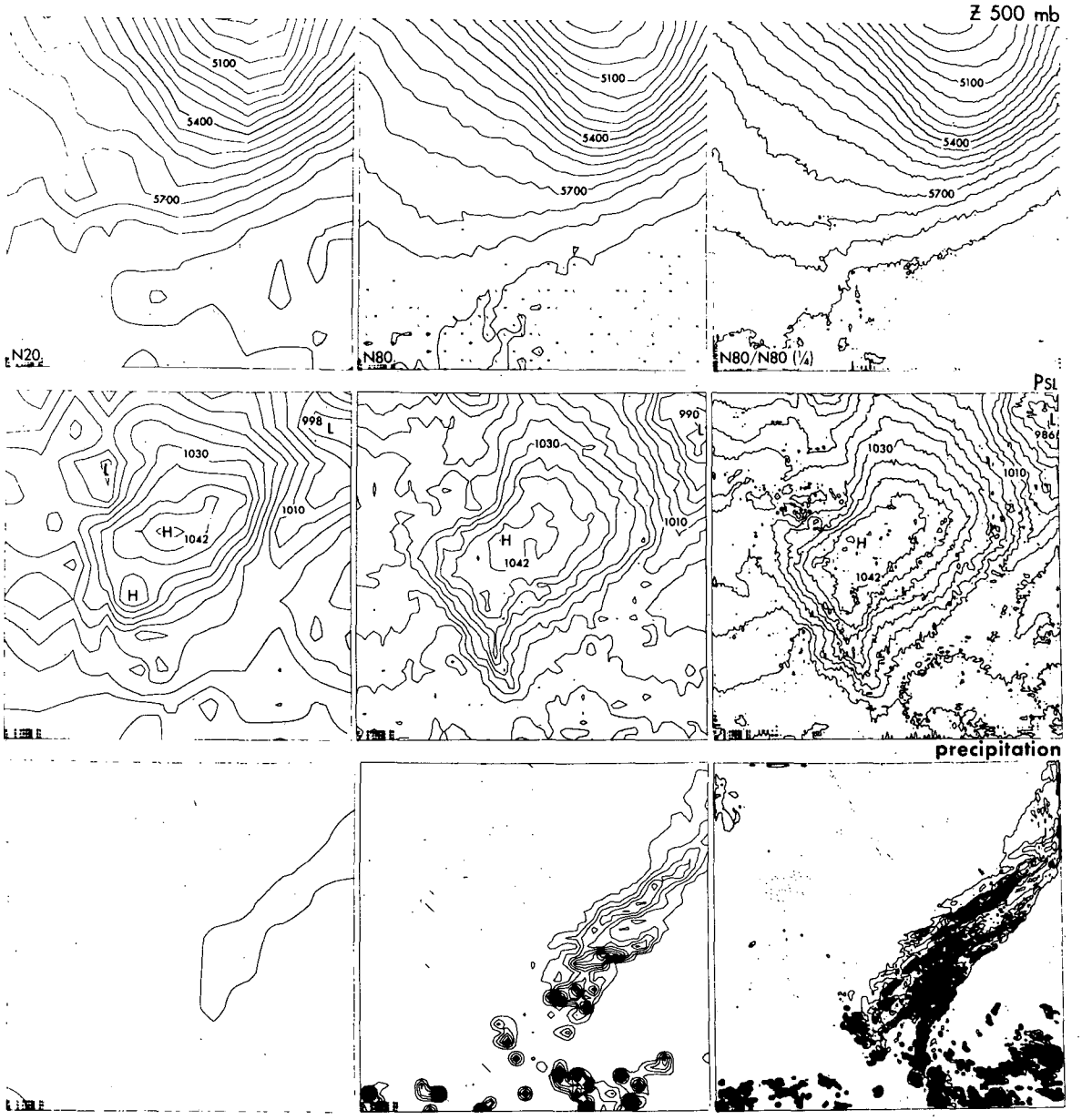

FIG. 12. The results of 1 day forecast with the *N*20 (left), *N*80 (middle) and *N*80/*N*80(1/4) (right) models. Upper: geopotential height (m) at 500 mb (*Z*500); contour interval is 60 m. Middle: sea level pressure P_{SL}. Lower: rate of precipitation; contour interval is 9.8 cm day^{-1}.

in the previous sections. The time step Δt for $N80/N80(1/4)$ model was 0.625 min. The leapfrog method was used throughout except the initial starting. The maps are for the geopotential height at 500 mb ($Z500$), the sea level pressure (P_{SL}), and the rate of precipitation. No cosmetic polish such as smoothing or filtering was applied whatsoever.

So far as the 1-day forecast is concerned, the $Z500$ maps are not essentially different from each other. The only differences are that eastward movement of the trough in $N20$ model is noticeably slow, and that the wiggles in the height patterns increase with the horizontal resolution. These wiggles are supposedly the internal gravity waves induced by the condensation heating vapor (the correspondence between the wiggles and the rain distribution was particularly clear at 0.5 day forecast maps). It is not certain, however, whether these disturbances were generated due to the right cause or due to the artificiality of the parameterization of the "moist convective adjustment."

The maps of the sea level pressure (P_{SL}) are relatively different among $N20$, $N80$ and $N80/N80(1/4)$ models. The higher resolution model [$N80/N80(1/4)$] has a larger difference in the pressure value between the high and the low centers than that in the $N80$-model. The kink in pressure pattern associated with the front (on the Eastern Seaboard) appears sharpest in the $N80/N80(1/4)$ resolution model.

A striking difference is found in the rate of precipitation. Fig. 12 reveals a considerable variation with the space resolution of the models. The maxima of the rain were 2.0 cm day^{-1} in $N20$, 15.2 cm day^{-1} in $N80$ and 35.0 cm day^{-1} in $N80/N80(1/4)$. In the 34 km mesh model, the detailed structure of two or three rainbands associated with a front may be observed. On the other hand, in the 135 km mesh model, these rains appeared as blocks of rain, and in the 540 km mesh model, the rain distribution was extremely crude. Note that in nature the two to three banded precipitation streakiness of 100 km width has been occasionally observed ahead of a warm front zone (e.g., Browning *et al.*, 1973).

The behavior of the rain patterns at the interface (boundary) area indicates that the treatment of interface condition worked properly. The $N80/N80(1/4)$ system has less problems at the interface than the $N20/N20$ system because of greater consistency between the coarse- and fine-mesh solutions.

Hovermale (1975) used a model of 60 km grid size and ten layers, and already reported that "considerable improvement in prediction accuracy (of rainfall) can be achieved through increased grid resolution." Hovermale's findings are very encouraging, and are supposed to be the recent breakthrough in numerical weather prediction. Our result seems to agree with that of Hovermale. However, he stated that "initial analysis and later boundaries play important, but secondary, roles in most limited area predictions." In this respect, our results suggest that this would not be the case even for 1 day forecasts, particularly if one takes a very small region.[3]

7. Conclusions

A three-dimensional, finite-difference, one-way nested grid model with full physics has been constructed, in which the ratio of the grid size between the coarse mesh in the large domain and the fine mesh in the small domain is 4:1. Three models (A, B and C) were tested; they include different formulations of lateral boundary treatment at the interface. The numerical solutions for all parameters in the fine-mesh model were compared with the solutions in the control model. The results revealed that the A- and C-models are satisfactory but that false reflections may sometimes occur at the interface between the small domain and the surroundings. The "sponge" scheme may produce an excessively smooth solution. The B-model, which included Orlanski's scheme of the "radiation condition," was useful in reducing the false reflection, though the removal was not complete. The treatment of the radiation condition for the flow at the σ-surface was not trivial; some adverse effects were experienced associated with the mountains along the interface. We have not developed entirely a method to obtain the most suitable treatment of this radiation condition.

It was shown that the major errors in all models come from the specified values at the interface (if the interface value is not accurate). The error contamination is rapid. For the limited domain covering the entire mainland of the United States, the error growth was not appreciable within 1 day but becomes sizeable in 2 days. In the A-, B- and C-systems, the errors remain less than the solutions of the homogeneously coarse-mesh model for 3 days. In particular, it was observed that with the interface condition tested here, nested models are effective for the parameters at the lower levels of the atmosphere and the rate of rainfall, but not effective for those in the stratosphere.

A combination of B- and C-systems (D-system) was applied to a 34 km mesh model with full physics. The integration was made up to 1 day without any difficulty. The detailed frontal structure and the rain bands associated with the front were calculated. The rain distributions turn out to be quite different among the models of 540, 135 and 34 km grid size, and the rain pattern in the finest resolution model was seemingly realistic.

---

[3] More recently Hovermale, Marks and Scolnik have reported, at the *Seventh Technical Exchange Conference* in El Paso, Tex., 1976, that "white higher resolution seems to be the key to improved forecasts, occasional inaccuracies in the new model suggest that more realistic initial conditions and lateral boundary input are also required."

Acknowledgments. The authors are thankful to Drs. J. H. Chen, Ta. Nitta, I. Orlanski and to Mr. R. Strickler for their stimulating discussions. Also, we wish to acknowledge the advice and criticism of Drs. J. Hovermale, I. Simmonds and A. Sundström, H. Davies, R. Elsberry, B. Hoskins, C. Kreitzberg, Y. Kurihara and the official reviewers. Gratitude is expressed to J. Chludzinski, J. Ryan, D. Hembree and K. Belnavis for their programming and technical assistance. We are indebted to Drs. J. Smagorinsky and W. Hess for their efforts to provide for a conducive research environment. Finally, thanks are given to Ms. Betty Williams for typing the manuscript.

REFERENCES

Anthes, R. A., 1974: Data assimilation and initialization of hurricane prediction models. *J. Atmos. Sci.*, **31**, 702–719.

Arakawa, A., and Y. Mintz, 1974: The UCLA atmospheric general circulation model. Notes for Workshop on the UCLA General Circulation Models of the Atmosphere and the Ocean, Dept. Meteor., University of California, Los Angeles, 120 pp.

Asselin, R., 1972: Frequency filter for time integrations. *Mon. Wea. Rev.*, **100**, 487–490.

Benwell, G. R. R., A. J. Gadd, J. F. Keers, M. S. Timpson and P. W. White, 1971: The Bushby-Timpson 10-level model on a fine mesh. U. K. Meteor Office Sci. Pap. No. 32, 35 pp. [Available from Meteorological Office, Bracknell, England.]

Bleck, R., 1973: Numerical forecasting experiments based on the conservation of potential vorticity on isentropic surfaces. *J. Appl. Meteor.*, **12**, 737–752.

——, 1974: Short-range prediction in isentropic coordinates with filtered and unfiltered numerical models. *Mon. Wea. Rev.*, **102**, 813–829.

Browning, K. A., M. E. Hardman, T. W. Harrold and C. W. Pardee, 1973: The structure of rainbands within a mid-latitude depression. *Quart. J. Roy. Meteor. Soc.*, **99**, 215–231.

Burridge, D. M., 1975: A split semi-implicit reformulation of the Bushby-Timpson 10-level model. *Quart. J. Roy. Meteor. Soc.*, **101**, 777–792.

Bushby, F. H. and M. S. Timpson, 1967: A 10-level atmospheric model and frontal rain. *Quart. J. Roy. Meteor. Soc.*, **93**, 1–17.

Chen, J. H., and K. Miyakoda, 1974: A nested grid computation for the barotropic free surface atmosphere. *Mon. Wea. Rev.*, **102**, 181–190.

Davies, H. C. 1976: A lateral boundary formulation for multi-level prediction models. *Quart. J. Roy. Meteor. Soc.*; **102**, 405–418.

Eliassen, A., and E. Raustein, 1968: A numerical integration experiment with a model atmosphere based on isentropic coordinates. *Meteor. Ann.*, **5**, 45–63.

Elsberry, R. L., 1975: Feasibility of an operational tropical cyclone prediction model for the western North Pacific area. U. S. Naval Postgraduate School, Tech. Rep. No. NPS-51Es 75051. [Available from Directory of Laboratory Programs, Dept. of the Navy, Washington, D. C. 20360.]

Elvius, T., and A. Sundström, 1973: Computationally efficient schemes and boundary conditions for a fine-mesh barotropic model based on the shallow-water equations. *Tellus*, **25**, 132–156.

Gall, R. L., 1976: Structural changes of growing baroclinic waves. *J. Atmos. Sci.*, **33**, 374–390.

Gambo, K., 1970: The characteristic features of medium-scale disturbances in the atmosphere (I) and (II). *J. Meteor. Soc. Japan*, **48**, 173–184, 315–330.

Hill, G. E., 1968: Grid telescoping in numerical weather prediction. *J. Appl. Meteor.*, **7**, 29–38.

Hoskins, B. J., and F. P. Bretherton, 1972: Atmospheric frontogenesis models: mathematical formulation and solution. *J. Atmos. Sci.*, **29**, 11–37.

Hovermale, J., 1975: Accuracy of prediction of heavy precipitation events in relation to grid resolution in numerical models. Briefing of performance of National Meteorological Center hurricane model at NOAA/NWS Hurricane Conference in Miami, 1975. [Available at NWC, Washington, D. C.]

Jones, D. E., 1974: The British Meteorological Office fine mesh, 10-level primitive equation model. *Notes from a Colloquium: Summary 1974 Subsynoptic Extratropical Weather Systems: Observation, Analysis Modeling and Prediction*, Vol. II, Seminar and Workshop at the National Center for Atmospheric Research, Boulder, Colorado, 394–408.

Kaplan, M. L., and D. A. Paine, 1973: A 32 km moist primitive equation model providing for scale interaction. *J. Atmos. Sci.*, **30**, 213–222.

Kessel, P. G. and F. J. Winninghoff, 1972: The Fleet Numerical Weather Central operational primitive-equation model. *Mon. Wea. Rev.*, **100**, 360–373.

Kreiss, H-O., 1968: Difference approximations for the initial-boundary value problem for hyperbolic differential equations. *Proc. Symp. Numerical Solutions of Nonlinear Differential Equations*, D. Greenspan, Ed., Wiley, 102 pp.

Kreitzberg, C. W., D. J. Perkey and J. E. Pinkerton, 1974: Mesoscale modeling forecasting and remote sensing research. Project THEMIS Final Rep. FCRL-TR-74-0253, Drexel University, 318 pp.

Manabe, S., J. Smagorinsky and R. F. Strickler, 1965: Simulated climatology of a general circulation model with a hydrologic cycle. *Mon. Wea. Rev.*, **93**, 769–798.

Matsumoto, S., S. Yoshizumi and M. Takeuchi, 1970: On the structure of the "Baiu-Front" and the associated intermediate-scale disturbances in the lower atmosphere. *J. Meteor. Soc. Japan*, **48**, 479–491.

Mesinger, F., 1973: A method for construction of second-order accuracy difference schemes permitting no false two-grid-interval wave in the height field. *Tellus*, **25**, 444–458.

——, and Z. I. Janjič, 1974: Noise due to time-dependent boundary conditions in limited area models. The GARP Programme on Numerical Experimentation, Rep. 4, 31–32.

Miyakoda, K., 1973: Cumulative results of testing a meteorological-mathematical model. The description of the model. *Proc. Roy. Irish Acad.*, **73**, 99–130.

——, R. F. Strickler, C. J. Nappo, P. L. Baker and G. D. Hembree, 1971: The effect of horizontal grid resolution in an atmospheric circulation model. *J. Atmos. Sci.*, **28**, 481–499.

Newton, C. W., 1954: Frontogenesis and frontolysis as a three-dimensional process. *J. Meteor.*, **11**, 449–461.

Nitta, T., and Y. Ogura, 1972: Numerical simulation of the development of the intermediate-scale cyclone in a moist model atmosphere. *J. Atmos. Sci.*, **29**, 1011–1024.

Okamura, Y., 1975: Computational design of a limited-area prediction model. *J. Meteor. Soc. Japan*, **53**, 175–188.

Oliger, J., and A. Sundström, 1976: Theoretical and practical aspects of some initial-boundary value problems in fluid dynamics. Tech. Rep., STAN-CS-76-578. Computer Sci. Dept., Stanford University.

Ookochi, Y., 1972: A computational scheme for the nesting fine mesh in the primitive equation model. *J. Meteor. Soc. Japan*, **50**, 37–48.

Orlanski, I., 1975: A rational subdivision of scales for atmospheric processes. *Bull. Amer. Meteor. Soc.*, **56**, 527–530.

——, 1976: A simple boundary condition of unbounded hyperbolic flows. *J. Comp. Phys.*, **21**, 251–269.

Pearson, R. A., 1974: Consistent boundary conditions for numerical models of systems that admit dispersive waves. *J. Atmos. Sci.*, **31**, 1481–1489.

Perkey, D. J., and C. W. Kreitzberg, 1976: A time-dependent lateral boundary scheme for limited-area primitive equation models. *Mon. Wea. Rev.*, **105**, 744–755.

Phillips, N. A., 1957: A coordinate system having some special advantages for numerical forecasting. *J. Meteor.*, **14**, 184–185.

Reed, R. J., and F. Sanders, 1953: An investigation of the development of a mid-tropospheric frontal zone and its associated vorticity field. *J. Meteor.*, **10**, 338-349.

——, and E. F. Danielsen, 1959: Fronts in the vicinity of the tropopause. *Arch. Meteor. Geophys. Bioklim.*, **A11**, 1–17.

Robert, A. J., 1966: The integration of a low-order spectral form of the primitive meteorological equations. *J. Meteor. Soc. Japan*, **44**, 237–245.

Sasaki, Y. K., 1970: Some basic formalisms in numerical variational analysis. *Mon. Wea. Rev.*, **98**, 875–883.

Shapiro, R., 1970: Smoothing, filtering and boundary effects. *Rev. Geophys. Space Phys.*, **8**, 359–387.

Shapiro, M. A., and J. J. O'Brien, 1970: Boundary conditions for fine-mesh limited-area forecasts. *J. Appl. Meteor.*, **9**, 345–349.

——, and J. T. Hastings, 1973: Objective cross-section analyses by Hermite polynomial interpolation on isentropic surfaces. *J. Appl. Meteor.*, **12**, 753–762.

Simmons, A. J., and B. J. Hoskins, 1976: Baroclinic instability on the sphere: normal modes of the primitive and quasi-geostrophic equations. *J. Atmos. Sci.*, **33**, 1454–1477.

Simons, T. J., 1972: The nonlinear dynamics of cyclonewaves. *J. Atmos. Sci.*, **29**, 38–52.

Smagorinsky, J., S. Manabe and L. Holloway, Jr., 1965: Numerical results from a nine-level general circulation model of the atmosphere. *Mon. Wea. Rev.*, **93**, 727–768.

Wang, H. H., and P. Halpern, 1970: Experiments with a regional fine-mesh prediction model. *J. Appl. Meteor.*, **9**, 545–553.

Williams, R. T., 1967: Atmospheric frontogenesis: A numerical experiment. *J. Atmos. Sci.*, **24**, 627–641.

Williamson, D. L., and G. L. Browning, 1974: Formulation of the lateral boundary conditions for the NCAR limited-area model. *J. Appl. Meteor.*, **13**, 8–16.

Wurtele, M. G., J. Paegle and A. Sielecki, 1971: The use of open boundary conditions with the storm-surge equations. *Mon. Wea. Rev.*, **99**, 537–544.